4 Qubit Rotations and Spin Nutations

Single qubit operations in spin quantum computing are spin nutations. They can be studied in a transient nutation experiment measuring the magnetisation of an ensemble. The transient nutation of a spin ensemble is described by the Bloch equations and was first observed in NMR by Torrey [1]. It is a well established technique in NMR and ESR, and was used to study, e.g. quadrupolar nuclei in disordered solids [2,3], or photo–induced paramagnetic species [4]. Here, the transient nutation method is used to study the decoherence during spin manipulation, and the behaviour of a S = 3/2 spin system with a fine structure such as N@C_{60} and P@C_{60}.

4.1 Experimental details

The pulse sequence used for the transient nutation experiment is presented in Fig. 4.1 (a). The first pulse, called the nutation pulse, rotates the spin depending on the pulse length t_p, as shown in Fig. 4.1(b). After a waiting time t, the spins are completely dephased and the remaining z component of the magnetisation is rotated by 90° with a second pulse so the signal can be measured in the x,y–plane. The full free induction decay (FID) after this pulse is recorded in order to extract the spectrum by FFT. The whole sequence is much shorter than the spin lattice relaxation time T_1 (chapter 3).

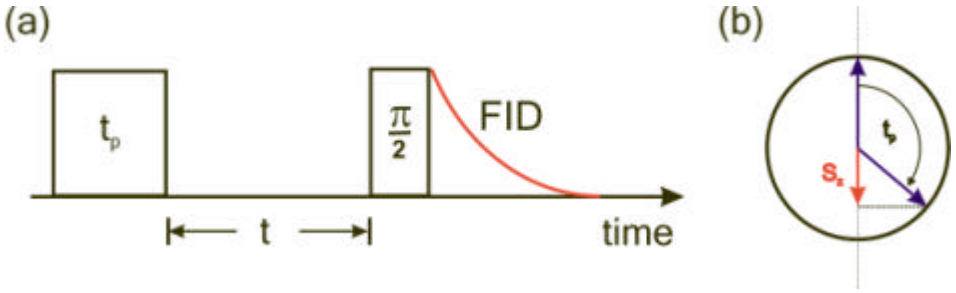

Fig. 4.1: (a) Scheme of the pulse sequence used for the transient nutation experiment. The spin rotation is driven by the first pulse. Its duration t_p is varied in the experiment. After the time t = 500 ns a p/2–pulse is applied measuring the z–magnetisation with an FID.

(b) Illustration of the spin rotation. The pulse duration t_p defines the rotation angle. Only the z–component S_z of the spin is measured. Depending on t_p it will oscillate between "up" and "down" position.

If the pulses of amplitude B_1 are applied in x–direction, the z component of the magnetisation remaining after nutation pulse t_p and waiting time t is rotated to the y–axis. For a two level system with isotropic g factor, and homogeneous linewidth as P@C_{60} and N@C_{60}, after an on–resonant excitation at t = 0 the ESR signal $S(t_p)$

$$S(t_p) \propto M_y(t_p) = M_z(0) \cdot \sin(w_1 t_p) \qquad (4.1)$$

is an oscillating function of the Rabi frequency w_1 that depends on the strength of the applied magnetic field B_1

$$w_1 = \frac{m_B g_e}{\hbar} B_1. \tag{4.2}$$

Here, $M_z(0)$ denotes the initial magnetisation, μ_B is the Bohr magneton, and g_e the Landé–factor of the electron. The excitation is on resonance if $w_{mw} = g_e b_e B_0/h$. For off–resonant excitation with a frequency shift $\Delta w = |g_e b_e B_0/h - w_{mw}|$, equation (4.1) has to be modified to [5]:

$$S(t_p) \propto M_y(t_p) = M_z(0) \cdot \frac{w_1}{w_{eff}} \cdot \sin(w_{eff} t_p) \tag{4.3}$$

with

$$w_{eff} = \sqrt{w_1^{\,2} + \Delta w^2}\,. \tag{4.4}$$

The effective nutation frequency w_{eff} observed for off–resonant excitation is therefore higher than the on–resonant nutation frequency w_1.

Spin–spin relaxation leads to an exponential decay of the signal and to [1,5]

$$M_y(t_p) = M_z(0) \cdot \frac{w_1}{w_{eff}} \cdot \sin(w_{eff} t_p) \cdot \exp\left(-\frac{t_p}{T_2} \left[1 - \frac{1}{2} \frac{w_1^{\,2}}{w_{eff}^{\,2}} \right] \right). \tag{4.5}$$

The spin–spin relaxation time T_2 can be shortened due to static inhomogeneities in B_0 and is then denoted as inhomogeneous relaxation time T_2^* (see also chapter 3). In the nutation experiment, additional inhomogeneities of B_1, especially for long pulse lengths t_p, further reduce the effective decoherence time T_2^*.

$N@C_{60}$ and $P@C_{60}$ are four level systems. Thus, their nutation is more complicated than for a simple two level system. For a detailed analysis of the nutation frequencies the essential couplings have to be taken into account. In our case these couplings are due to the hyperfine interaction and the zero–field splitting, respectively.

$$H_{coup} = a\mathbf{IS} + \mathbf{SDS} \tag{4.6}$$

The hyperfine interaction $H_{hf} = a\mathbf{IS}$ of group–V endohedral fullerenes is isotropic (see chapter 2). In this case the nutation frequency does not depend on the hyperfine coupling and the nutation frequency is expected to be $w_{nut} = w_1$ for nitrogen and phosphorous in C_{60} [5].

Two cases have to be considered when measuring the nutation frequency [5,6]:

$$w_{nut} = \overbrace{\begin{cases} w_1 & |H_1| >> |SDS| \\ 2w_1 & |H_1| << |SDS| \end{cases}}^{for\ (1/2,-1/2)\ transitions} \text{ and } w_{nut} = \overbrace{\begin{cases} w_1 & |H_1| >> |SDS| \\ \sqrt{3}w_1 & |H_1| << |SDS| \end{cases}}^{for\ (\pm 3/2,\pm 1/2)\ transitions} \tag{4.7}$$

Here, H_1 is the force of the driving microwave with $H_1 = 2g_e\mu_B \boldsymbol{B}_1 \boldsymbol{S}$. For an S = 3/2 system, the term $|SDS| = |D|$.

In ESR spectroscopy of complex materials, advanced transient nutation methods exist such as the rotary echo [7] or one and two dimensional PEANUT sequences [8]. These are used to cancel effects of inhomogeneities of the magnetic fields and to simplify the signals of complicated spectra. For quantum computing, it is of interest to keep the pulse sequences as simple and as short as possible. Therefore, we use the simplest possible version of the nutation experiment as shown in Fig. 4.1.

4.2 Nutation and Selectivity

For quantum computing one– and two–qubit gates should be fast and the qubits should have small decoherence at room temperature, if possible. Fast operations on single qubits, e.g. fast single spin rotations, require strong magnetic fields and short pulses respectively, as can be seen from equation (4.2). The spin–spin relaxation time of N@C_{60} is T_2 = 20 µs even at room temperature, so with pulse lengths of ~ 20 ns up to 1000 rotations or quantum operations could be possible.

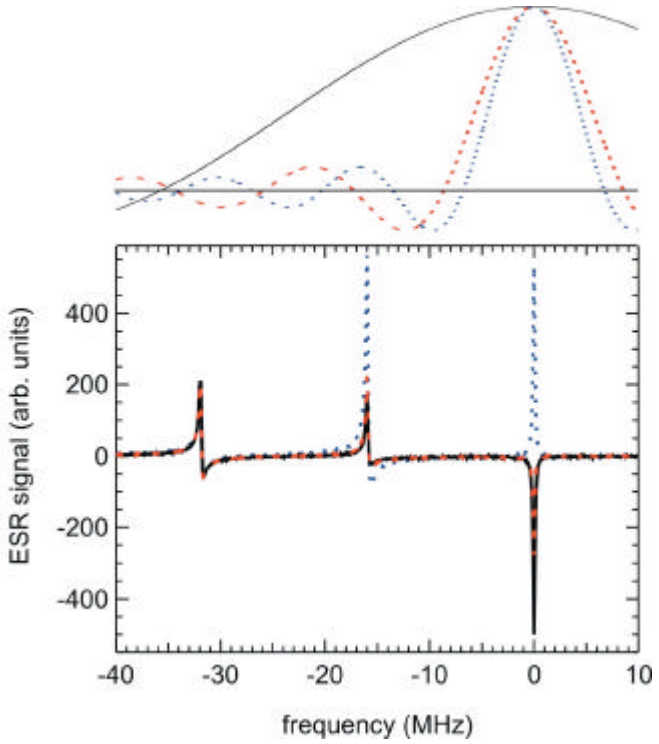

Fig. 4.2: Spectra after the nutation pulse sequence with pulse lengths t_p = 28 ns (black line), t_p = 116 ns (red dashed line), and t_p = 148 ns (blue dotted line) was applied at the m_I = 1 hyperfine line (low field). The sinc functions corresponding to the pulse lengths are shown in the upper part of the figure.

However, the spectrum of an N@C_{60} ensemble consists of three hyperfine lines with an isotropic hyperfine coupling constant a = 16 MHz (chapter 2). Pulses are rectangle functions in the time domain of width t_p and therefore sinc–shaped in the frequency

domain with the first zero–crossing at $1/t_p$. This means that short pulses will affect more than one hyperfine line.

In Fig. 4.2, the effect of the pulse sequence in Fig. 4.1(a) on the nitrogen spectrum is shown for t_p = 28 ns (black line), t_p = 116 ns (red line), and t_p = 148 ns (blue line). Because of the long coherence time T_2 = 20 µs of the nitrogen spins, the time between the pulses had to be as long as t = 12 µs. The length of the "read-out"–pulse was $t(\pi/2)$ = 24 ns. The spectra shown in Fig. 4.2 were obtained after Fourier transformation of the following FID.

From the spectra we can see that both, the $m_I = 1$ and the $m_I = 0$ hyperfine line, are affected by the nutation pulse. Only the $m_I = -1$ hyperfine line remains the same. Therefore, in the following data analysis, the nutation cannot be taken from the bare FID because it contains the information of all three hyperfine lines and their oscillation. Instead, the oscillation of the on-resonant point of the $m_I = 1$ hyperfine line has been evaluated.

The pulse sequence form Fig. 4.1(a) was applied for many different pulse lengths t_p. The data obtained in this experiment are shown in Fig. 4.3 (black markers). In combination with the fit to equation (4.5) (red line), they reveal the Rabi oscillation of the S_z component as illustrated in Fig. 4.1(b).

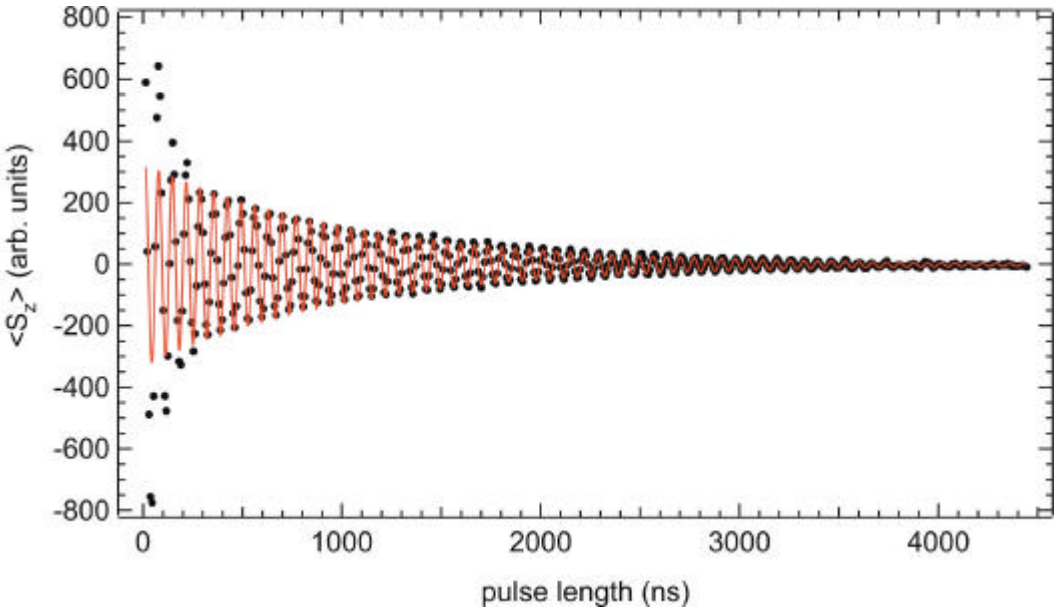

Fig. 4.3: Transient nutation of the $m_I = 1$ hyperfine line of $N@C_{60}$ in solid state at room temperature. The data points (black markers) have been fitted by a sine function with an exponential decay (red line) after equation (4.5). This decay is due to inhomogeneities of the applied magnetic fields B_0 and B_1 (see text).

The decay of the signal is due to T_2^* relaxation. Since this is expected to follow an exponential function, the first data points seem much higher than expected. Obviously, the decay of the signal gets slower with increasing nutation pulse length. In other words, the spin–spin relaxation time changes with the selectivity of the pulses.

Non–selective pulses affect all spins of the entire ensemble. If selective pulses are applied, only a part of the spin ensemble is measured. In this case, the variation of the Lamor–frequency over the probed ensemble is smaller, and hence the apparent spin–spin relaxation is slower than for non–selective pulses.

Nevertheless, the fit reveals only one nutation frequency $w_{nut}/2\pi = w_1/2\pi$ = 14.5 MHz. With equation (4.2), this corresponds to a magnetic field in the sample of B_1 = 0.52 mT. The relaxation time obtained by the fit is T_2^* = 1 µs, The relaxation time obtained by the fit is T_2^* = 1 µs, which is just the relaxation time of the FID. Thus, if a Hahn–Echo sequence were used instead of a single π/2–pulse and inhomogeneities of B_1 are negligible, the limit of T_2 = 20 µs as obtained in chapter 3 should be reached.

The hyperfine coupling constant of atomic phosphorous in C_{60} is $a/2\pi h$ = 138 MHz (chapter 2). In contrast to N@C_{60}, even short pulses with t_p ~ 12 ns can be applied selectively on one hyperfine line. Therefore, the experiment described for N@C_{60} has been applied for P@C_{60} with larger magnetic field B_1 and a "read–out"–pulse with t(π/2) = 12 ns. Due to the shorter spin–spin relaxation time of P@C_{60} (chapter 3), the time between the pulses has been chosen as t = 1 µs.

In Fig. 4.4 (a) the data (black markers) and the fit (red line) are shown. The data have been multiplied with an exponential function exp(x/500 ns) for better illustration. As for nitrogen, the relaxation time increases with the length of the nutation pulse until a pulse length of t_p ~ 150 ns is reached. The nutation frequency obtained from the fit is $\omega_{nut}/2\pi$ = 22.1 MHz corresponding to a field B_1 = 0.8 mT.

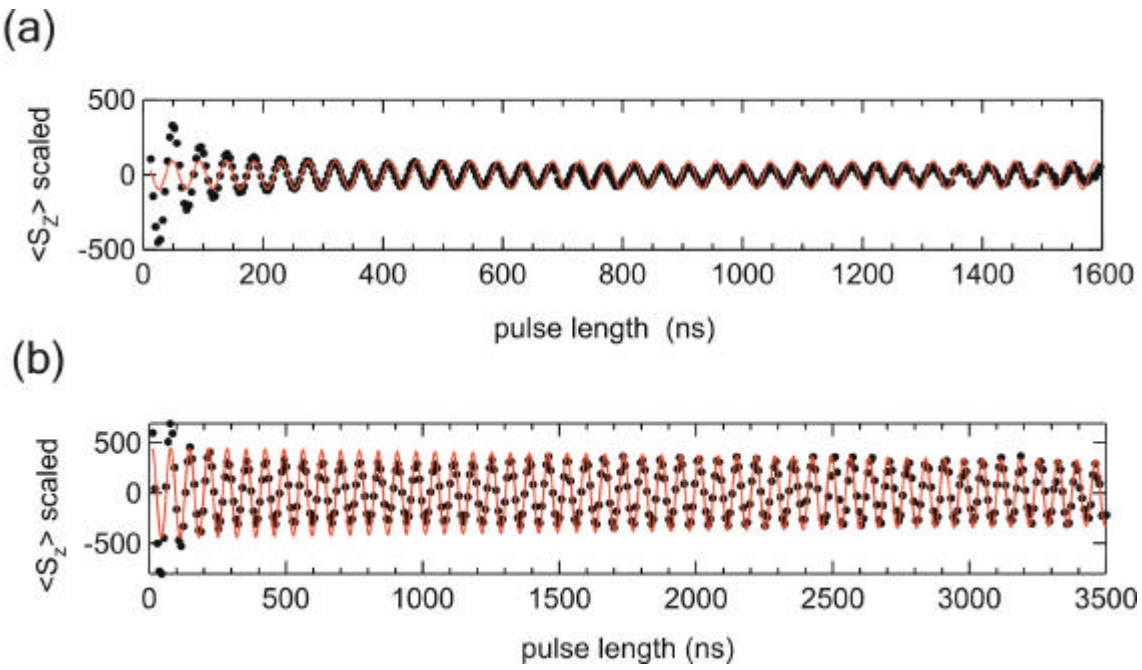

Fig. 4.4: (a)Data (black markers) and fit (red line) of the transient nutation experiment with P@C_{60}. The applied magnetic field was B_1 = 0.8 mT. data are multiplied with exp(x/500 ns).

(b)Nutation of N@C_{60} and fit from Fig. 4.3 multiplied with exp(x/1100 ns). The applied magnetic field was B_1 = 0.52 mT. Note that the x scale is different from fig. (a).

For comparison, the data and the fit of Fig. 4.3 scaled by exp(x/1100 ns) are shown again in Fig. 4.4 (b). Though the conditions are not ideal, more than 50 oscillations for N@C_{60} and about 30 oscillations for P@C_{60} can be observed. This means that at least 50 (30) single qubit operations can be done at room temperature. For short QC gates (e.g. a two–qubit CNOT) this is sufficient. Therefore, QC pulse sequences can be done without refocusing and thus can be kept shorter and simpler than in liquid NMR.

4.3 Nutation of P@C_{60} (solution)

In chapter 2 we found that three different transitions can be observed in a single hyperfine line for P@C_{60} in solution due to second order hyperfine splitting. In order study the influence of this splitting on single qubit rotations, the transient nutation of P@C_{60} in solution has been studied. As the molecules rotate very fast in the solvent, all dipolar interactions, in particular the zero–field splitting, are averaged out. So, the hyperfine coupling is the only interaction remaining.

The pulse sequence of Fig. 4.1 has been applied on the hyperfine line $m_I = 1/2$ with $t(\pi/2) = 16$ ns, a waiting time t = 500 ns, and an applied field $B_1 = 0.79$ mT.

Similarly to N@C_{60}, the experiment revealed only one nutation frequency $\omega_{nut}/2\pi = 21.7$ MHz (Fig. 4.5(a)) corresponding to an applied field $B_1 = 0.78$ mT indicating that the field inside the sample is nearly the same as outside.

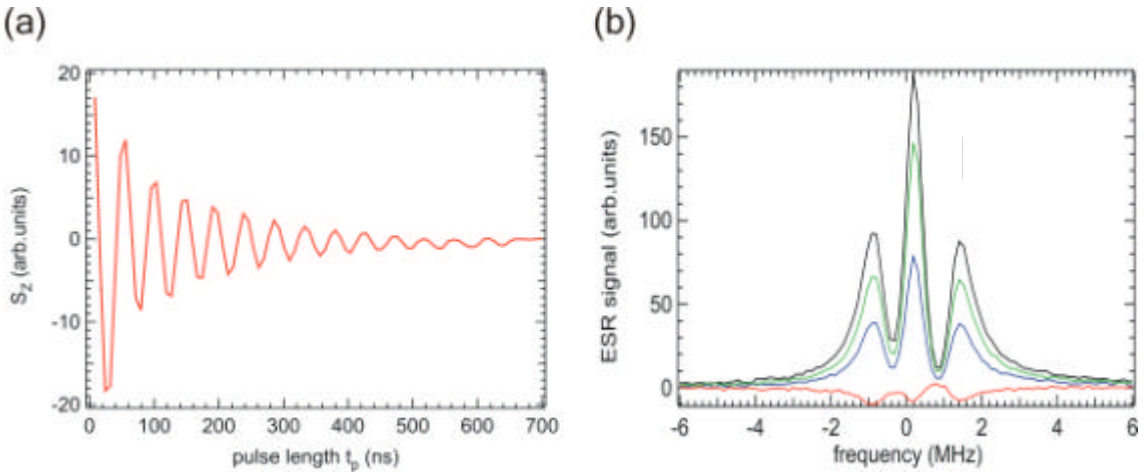

Fig. 4.5: (a) Transient nutation of P@C_{60} in solution at room temperature. The nutation frequency of $w_{nut}/2p$ = 21.7 MHz corresponds to a field B_1 = 0.775 mT. The oscillations observed belong to the integrated signal of the centre line of the fine structure triplet at m_I = 1/2.

(b) Spectrum of P@C_{60} during the first oscillation of the transient nutation in (a) at t_p = 8 ns (black), t_p = 16 ns (blue), t_p = 32 ns (red), and t_p = 48 ns (green). The nutation pulse affects all transitions in the same way.

In Fig. 4.5 (b) the spectrum of P@C_{60} in solution is shown for different nutation pulse lengths t_p. The centre line corresponds to the (1/2,-1/2) transition, the outer lines to the (±1/2, ±3/2) transitions respectively. All transitions are affected equally during the first oscillation. This is nearly the same during the whole experiment, because even at pulse

lengths as long as t_p = 700 ns, the frequency width of the nutation pulse covers the all finestructure lines. In this case the S = 3/2 system can be treated as a simple single qubit.

In order to observe differences in the nutation of the different transitions, the applied field and therefore the nutation frequency has to be smaller than the splitting of ~ 1 MHz. This has been done in the measurement shown in Fig. 4.6. It reveals a very small Rabi frequency of $w_{nut}/2\pi$ = 0.3 MHz for the (1/2,-1/2) transition corresponding to a field B_1 = 0.011 mT. After a Fourier transformation of the Rabi oscillation, components with higher frequencies become visible. A strong contribution of the 1 MHz off–resonant (±3/2, ±1/2) transitions is shown in the inset of Fig. 4.6 with $w_{eff}/2\pi$ = 1 ± 0.25 MHz in agreement with equation (4.4).

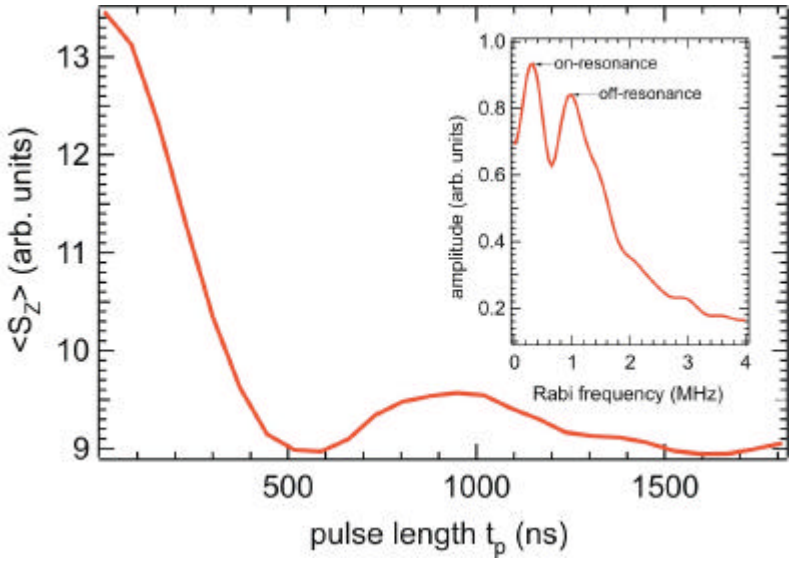

Fig. 4.6: Transient nutation of P@C_{60} at B_1 = 0.011 mT. The oscillation observed belongs to a single point of the centre line of the fine structure triplet at m_I = 1. The inset shows the Fourier transform of the signal that contains two peaks. The first at $w/2p$ ~ 0.3 MHz corresponding to the nutation frequency of the (1/2,-1/2) transition, the second at $w/2p$ ~ 1 MHz corresponding to the off resonant components of the (±1/2,±3/2) transitions.

No change in the nutation frequency corresponding to $w_{nut} = 2 \cdot w_1$ (for the (1/2,-1/2) transition) or $w_{nut} = \sqrt{3} \cdot w_1$ (for the (±3/2, ±1/2) transitions) could be observed. This is consistent with the fact that the hyperfine coupling is isotropic [5]. However, if small driving fields are used in a quantum computing sequence, the off–resonant qubit rotations have to be taken into account.

4.4 Nutation of P@C_{60} (powder)

One striking difference between nitrogen and phosphorous in C_{60} at room temperature is that for the latter only the (1/2,-1/2) transitions are visible in the spectrum. This may have its origin in a powder broadening of the other transitions due to a large zero–field splitting H_{fs} = **SDS**.

A transient nutation experiment can reveal the influence of the fine structure Hamiltonian because the nutation frequency w_{nut} depends on the matrix element of the $S_{\pm}$ operator for the spin transition [5]. The nutation frequency w_{nut} of the (1/2,-1/2) transition will be $w_{nut} = 2 \cdot w_1$ for $2g_e\mu_B B_1 << |D(\vartheta)|$ with $|SDS| = |-1/3\ D(\vartheta)S^2 + S_z^2\ D(\vartheta)| = |m_s^2 - S(S+1)/3| \cdot |D(\vartheta)|$ (for details see discussion in chapter 5), according to equation (4.7). For $2g_e\mu_B B_1 >> |D(\vartheta)|$ it will be equal to the field induced frequency w_1 from equation (4.2) with $w_{nut} = w_1$ as discussed before. If the transient nutation of this spin transition is measured as a function of B_1, the value of D can be estimated.

From Dinse et al. [9] it is known that in N@C_{60}, D is in the order of $D/g_e\mu_B \sim 20$ µT. Thus, in a sufficient B_1 regime, the condition $2g_e\mu_B B_1 >> |D(\vartheta)|$ will be valid and N@C_{60} can be used as a standard for the B_1 strength. In Fig. 4.7, the nutation frequency of a N@C_{60} powder sample is shown as a function of the applied field B_1. As expected, it is a straight line through zero, so indeed this sample is a good standard in this B_1 regime.

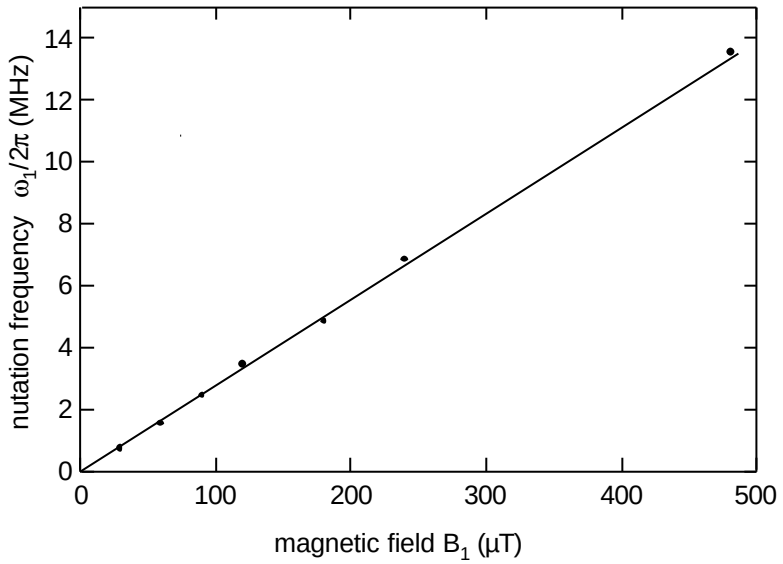

Fig. 4.7: Nutation frequency of N@C_{60} as a function of the magnetic field B_1. The magnetic field was calculated from the nutation frequency for the highest point and then has been scaled down by the attentuation. The points are lying on a straight line through origin, indicating that the frequency w_1 can be used as a standard for the B_1 strength.

Due to the isotropic hyperfine interaction, there is no influence of the different nuclear spins I = 1 for nitrogen and I = 1/2 for phosphorous on the nutation frequency [5,10]. Therefore, the nutation frequencies of the different samples can be compared directly.

The nutation frequencies w_{nut} of two P@C_{60} powder samples of different spin concentration, "Pharao" and "Phobos", have been investigated at room temperature. The ratio of filled to empty fullerene molecules is $1 \cdot 10^{-6}$ for the further and $1.6 \cdot 10^{-4}$ for the latter sample. Again, the pulse sequence of Fig. 4.1 has been used. The time between the pulses was t = 1µs, the length of the "read–out" pulse has been adjusted to the field strength in order to get the maximum signal.

In Fig. 4.8, the nutation of the on-resonance point of the m_I = 1/2 hyperfine line "Pharao" (dashed red line) is compared with the nutation of N@C_{60} (black line) at different strengths of B_1.

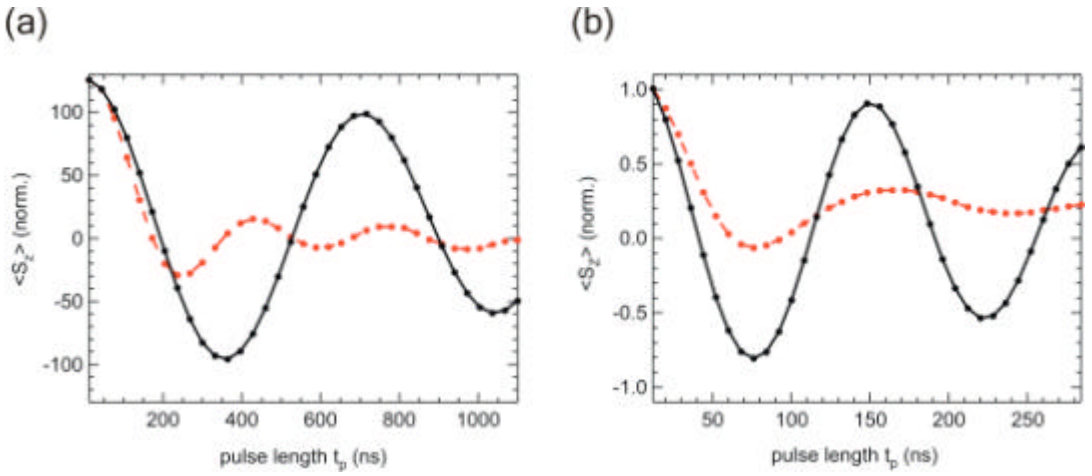

Fig. 4.8: Nutation of "Pharao" (dashed red line) and N@C_{60} (black line) at (a) B_1 = 60 µT with 32 ns steps in pulse length and (b) B_1 = 240 µT with 16 ns steps.

At B_1 = 60 µT (see Fig. 4.8(a)), the nutation frequency of the phosphorous sample is twice as high as the nutation frequency of the nitrogen sample. In contrast, Fig. 4.8(b) shows that at B_1 = 240 µT, the nutation frequencies of both samples are nearly the same. A small deviation can be explained with the slight deviation of B_1 in "Pharao" compared to the "Nike" standard.

For both phosphorous samples, "Pharao" and "Phobos", the ratio of w_{nut}/w_1 as a function of B_1 is shown in Fig. 4.9, where w_1 is the "standard" nutation frequency taken from Fig. 4.7. The Fourier transform (with Hanning window) of the nutation reveals the ratio ~ 1 for B_1 > 240µT and ~ 2 for B_1 < 60µT, independent from the amount of filled fullerene molecules which is 160 times as high in "Phobos" compared to "Pharao". The deviation from the integer numbers is due to slightly smaller B_1 fields in the phosphorous samples compared to the N@C_{60} sample.

Between B_1 = 240 µT and B_1 = 60 µT, two main frequency contributions, $w_{nut} = w_1$ and $w_{nut} = 2 \cdot w_1$, are always visible. This is due to the powder distribution of the angle dependent SDS term. It can be treated as a dipolar coupling (see chapter 5) with $D(\vartheta) = D_0 \cdot (3\cos^2\vartheta - 1)$, with ϑ the angle of the main axis of D with respect to B_0.

In a powder sample, all angles are present and therefore, couplings as strong as $2 \cdot D_0$ can be measured, which fulfil $D_0 >> g_e \mu_B B_1$ for rather strong magnetic fields. Spins belonging to this sub–ensemble show the nutation frequency $w_{nut} = 2 \cdot w_1$. However, there is always a number of spins with $D(\vartheta) < 2 g_e \mu_B B_1$ present, too. Especially the nutation frequency of those spins with $|D(\vartheta)| = 0$ will be w_1 for every applied B_1. This explains why in Fig. 4.9 (b) – (f), both nutation frequencies are measured. The sub–ensemble with $|D(\vartheta)| < 2 g_e \mu_B B_1$ gets smaller with decreasing B_1, while the number of

spins with $|D(\vartheta)| >> 2g_e\mu_B B_1$ increases shifting the intensity of the peaks from w_1 towards $2w_1$.

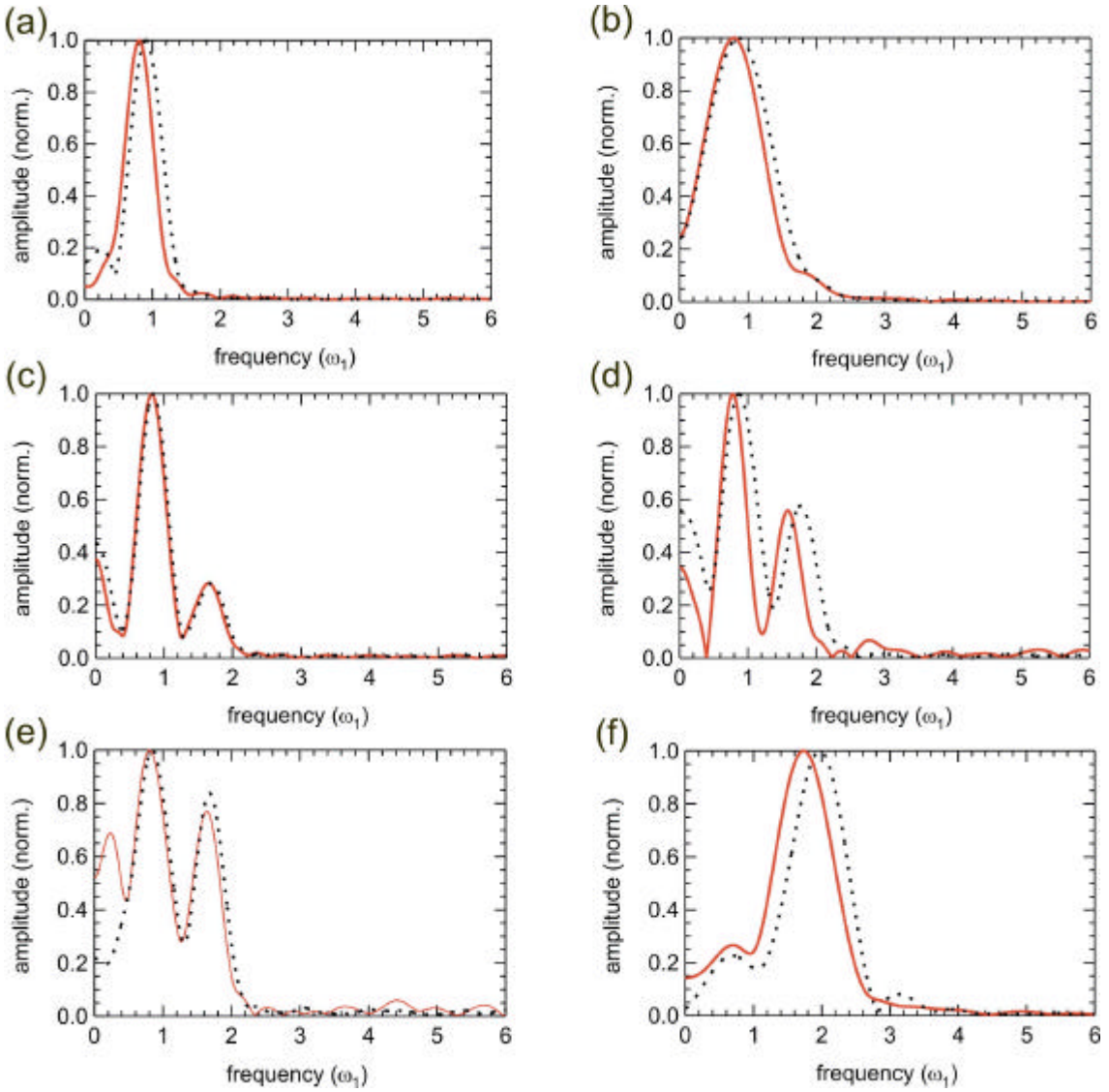

Fig. 4.9: The nutation frequency spectrum of the P@C_{60} samples "Pharao" (solid red line) and "Phobos" (dashed black line) at room temperature for different magnetic fields B_1, (a) B_1 = 480 µT, (b) B_1 = 240 µT, (c) B_1 = 180 µT, (d) B_1 = 120 µT, (e) B_1 = 90 µT, and (f) B_1 = 60 µT. The frequency axis is labelled in units of the N@C_{60} nutation frequency w_1 corresponding to the applied field.

Nutation frequencies $2 \cdot w_1$ arise when B_1 = 240 µT (Fig. 4.9 (b) to (f)). This contribution belongs to those spins that have the strongest coupling possible with $2g_e\mu_B B_1 << 2 \cdot D_0$. Hence, a zero–field splitting of $D_0/g_e\mu_B \sim 240$ µT can be estimated.

Two clearly distinct lines are observed in the nutation spectra for B_1 = 240 µT, no matter of the exact value of B_1. The "complicated behaviour" of the nutation frequencies for $H_1 \approx$ **SDS** as predicted in [5] is not resolved in these experiments. This might be due to the bad frequency resolution of pulsed experiments. For a more detailed investigation

of this point, a low power experiment would be necessary in order to detect the spin nutation during the B_1 pulse.

Turning back to the question whether the zero–field splitting can explain the vanishing of the second order hyperfine structure in solid P@C_{60} at room temperature, we find that the value $D_0/g_e\mu_B$ ~ 240 µT is much too small to explain the strong broadening of the lines. An additional, large non–axial term $E/2g_e\mu_B$ ~ 600 µT in the zero–field splitting could explain the observed huge line broadening. But this would be contradictory to the almost spherical symmetry of solid C_{60} at room temperature. Thus, a fast relaxation of the (±3/2, ±1/2) transitions has to be considered as the reason for the vanishing lines.

With decreasing temperature both relaxation times, T_1 and T_2, increase (see chapter 3). If the (±3/2, ±1/2) transitions are invisible due to fast relaxation at room temperature, measurements at low temperatures might give more insight. In Fig. 4.10, the nutation for the low field hyperfine line of the sample "Phobos" at T = 10 K is shown. The applied field has been chosen very small with B_1 = 9 µT to be as selective as possible with the "read–out"–pulse t(π/2) = 480 ns. In contrast to the above measurements, we did not choose to observe the oscillation of a single point of the spectrum. Instead, the integrated intensity of the FID has been measured in order to increase the signal to noise ratio.

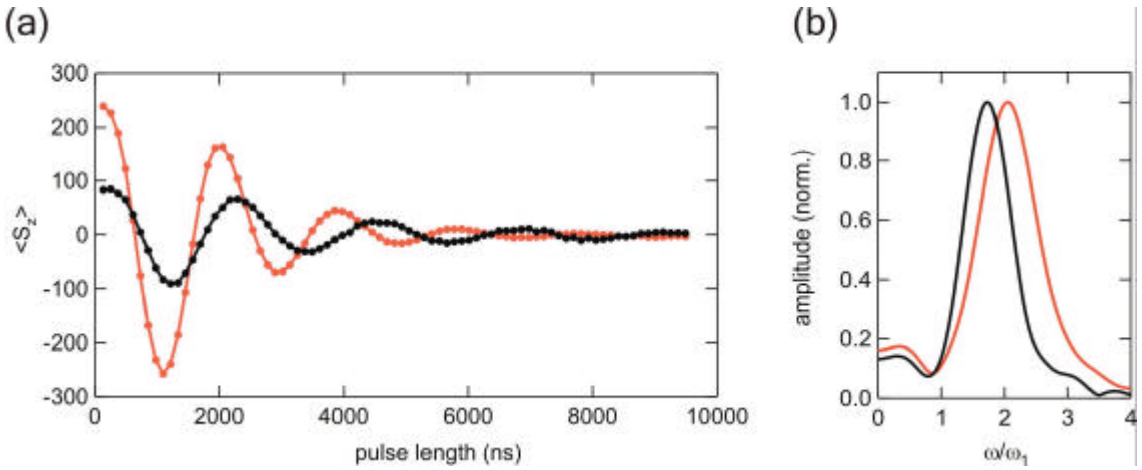

Fig. 4.10:(a)Transient nutation at T = 10 K and B_1 = 9 µT of the sample "Phobos". The usual pulse sequence has been applied at the m_I = 1/2 hyperfine line. The red line shows the nutation of the (1/2,-1/2) transition, the black line shows the same measurement at 0.5 mT off–resonant excitation.

(b)The Fourier transformation of the nutation reveals clearly the ratio of the frequencies. For the (1/2,-1/2) transition $w_{nut} = 2^{½}w_1$, and for the outer finestructure line it is $w_{nut} = v3^{½}w_1$ as expected for the (±3/2, ±1/2) transitions.

If B_0 is chosen on resonance with the (1/2, -1/2) transition (red line), the nutation frequency is $w_{nut}/2\pi$ = 0.52 MHz = $2w_1/2\pi$, exactly as expected[9]. The black line shows the nutation at 0.5 mT off–resonant excitation with $w_{nut}/2\pi$ = 0.44 MHz = $\sqrt{3}\cdot w_1/2\pi$ as expected for the (±3/2, ±1/2) transitions. In Fig. 4.10 (b), the Fourier transform (with Hanning window) of the nutation signals proves that the accuracy of the measurement is good enough to resolve the different frequencies.

As mentioned before, the signal of the the (±3/2, ±1/2) transitions seems to vanish at room temperature. However, at T = 10 K and B_1 = 9 µT, echo detected spectra as in Fig. 4.11 (black line) reveal the fine structure triplet. There are reports about similar structures measured at low temperatures (10 K – 80 K) in W-Band experiments [6].

The simulation (red line) shows that the centre line is of Lorentzian shape. A zero–field splitting of $D_0/g_e\mu_B$ = 650 µT has been assumed for the outer lines that are supposed to have the same width as the centre line (100 µT). The intensity ratio of the lines in the simulation is 3:4:3 as expected for dipolar interaction [[4]]. The large D value is supported by nutation experiments at T = 10 K similar to those shown in Fig. 4.9, where frequencies of $2w_1$ already contribute at B_1 = 400 µT.

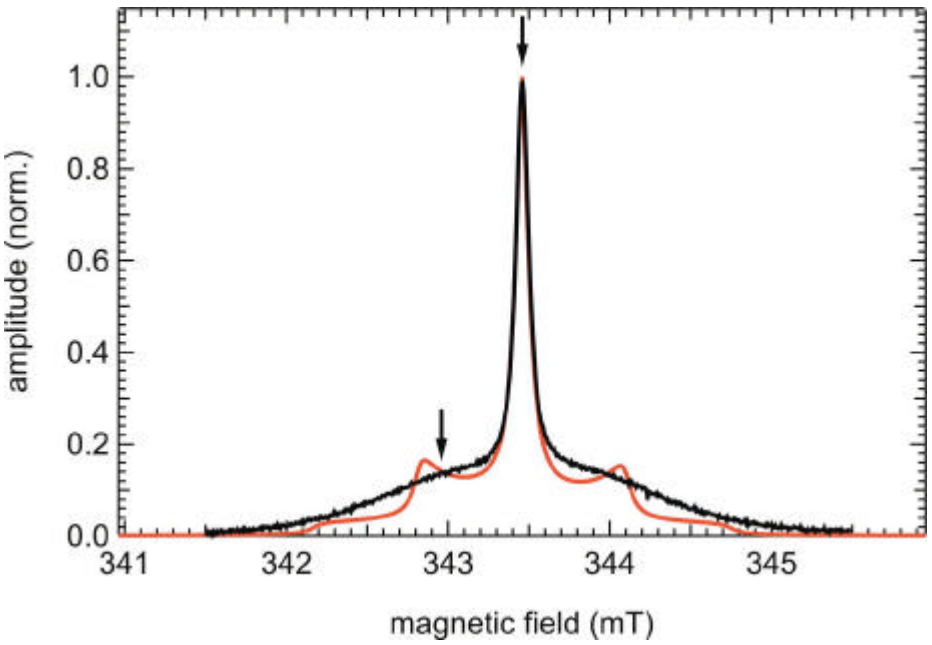

Fig. 4.11: Echo detected spectrum of the low field hyperfine line of the powder sample "Phobos" at T = 10 K and B_1 = 9 µT (black line). The spectrum has been simulated with a linewidth of 100 µT and a splitting of $D/g_e\mu_B$ = 650 µT (red line). Only a large distribution of D splittings can explain the strong broadening of the (±3/2, ±1/2) transitions (see text). The arrows indicate the positions, where the spin–spin relaxation and the nutation shown in Fig. 4.10 have been measured selectively.

[9] The nutation at large magnetic field, B_1 = 646 µT >> $D/2g_e\mu_B$ ($\omega_1/2\pi$ = 18.1 MHz), has been used as reference. To reach B_1 << $D/2g_e\mu_B$, an attenuation of 37 dB has been used.

Selective measurements[10] of the spin–spin relaxation yield T_2 = 3 µs for the (1/2, -1/2) transition at B_0 = 343.46 mT and T_2 = 4 µs at B_0 = 342.96 mT. The delay time between the two echo pulses has been t = 3 µs. Therefore, the longer relaxation time of the outer lines is the reason for the higher intensity of these lines compared to the centre line.

In contrast to the spin–spin relaxation, the spin–lattice relaxation time T_1 = 1.3 ms is much shorter at the off–resonant position B_0 = 342.96 mT than at the (1/2, -1/2) transition, where two relaxation times can be measured, T_1 = 25 ms and T_1 = 5 ms. These times are very long compared to the pulse sequence, so no influence on the line shape is expected.

The strong line broadening of the (±3/2, ±1/2) transitions could be due to anisotropic dipolar interaction of the endohedral spin with a ^{13}C atom on the fullerene molecule. Indeed, a small anisotropic dipolar coupling of ^{13}C with the endohedral atom has been observed for N@C_{60} [9,13]. However, if the linewidth of the centre line is assumed to be due only to dipolar coupling with adjacent spins, the (±3/2, ±1/2) transitions are expected to be three times broader. Even then, the simulation would not fit the data. To sum up, neither relaxation effects nor dipolar interactions can explain the line broadening.

A strong broadening that affects only the (±3/2, ±1/2) transitions can be explained by a distribution of D values. This can have two different origins:

X–ray diffraction measurements of pure C_{60} crystals revealed a non-uniform charge-density distribution on the C_{60} cage induced by crystal-field effects (see [14] for a nice review). Such a deformation of the fullerene cage causes a zero–field splitting of the endohedral spin, as observed in liquid crystal experiments with N@C_{60} (this will be discussed in detail in chapter 5). A distribution of the magnitude of such deformations would cause a distribution of D values. It is likely that there are different crystal–fields in a powder sample. Especially, a difference between bulk and surface material has to be expected. But to result in such a broad distribution as indicated by the spectra, the distribution of cage distortions has to be of the same order of magnitude as the effect of the distortions on the endohedral atom.

Alternatively, a variation of off–centre positions of the phosphorous atom in the C_{60} cage could provide another explanation of a broad, Gaussian distribution of D values. Some calculations [25,26] predict an off–centre position of the endohedral phosphorous atom due to a change of symmetry or a flat potential inside the fullerene molecule. However, in both cases the hyperfine coupling would be expected to be anisotropic. No evidence for anisotropic interactions has been found experimentally. This supports the calculations that show a centre–position of the phosphorous atom [23,24]. Thus, it seems that the amorphous or nano–crystalline structure of the powder samples is the reason for the distribution of D values.

[10] The frequency width of the π–pulse has been $\Delta\omega_1/2\pi$ = 2.27 MHz corresponding to ΔB_1 = 80 µT.

Irrespective of its origin, the distribution of D values would be averaged out at room temperature due to the fast rotation of the C_{60} molecules. Thus, one would expect to see a three line powder spectrum similar to the simulation in Fig. 4.11. Indeed, the nutation experiments at room temperature indicate an averaging of the zero–field splitting (zero–field splitting) to a smaller D value. But only T_2 relaxation can be responsible for the "vanishing" of the finestructure lines.

For P@C_{60} in solution, it is known that the modulation of the zero–field splitting is the main spin–spin relaxation mechanism [19]. With decreasing temperature the correlation time increases, and the (±3/2, ±1/2) transitions get broader. At T = 163 K the outer lines of the finestructure triplet cannot be resolved anymore.

The rotation of the C_{60} molecules in a powder sample may lead to a modulation of the zero–field splitting. For correlation times $\tau_c \sim 32$ ps the (±3/2, ±1/2) transitions will vanish completely. These rotations freeze out at T = 80 K, the zero–field splitting is not modulated anymore, and the transitions are again observed.

4.5 Conclusions

Fast spin nutations and therefore fast single qubit operations require short pulses and strong magnetic fields, respectively. As shown, different aspects have to be taken into account when trying to operate P@C_{60} and N@C_{60} as qubits:

Because of the large hyperfine coupling constant of P@C_{60}, pulses applied on–resonance on one hyperfine line will always be selective on this transition. In contrast, the distance between the outmost hyperfine lines of N@C_{60} is only 1.12 mT. It has been shown that with an on–resonance applied magnetic field of $B_1 \sim 0.5$ mT on one of the outer hyperfine lines, the other outermost hyperfine line remains completely unaffected.

The hyperfine coupling is completely isotropic for both of the endohedral fullerenes. As discussed, the hyperfine interaction has therefore no influence on the intrinsic nutation frequency and all hyperfine lines are affected equally by a strong enough pulse.

In solution, the three different transitions of a single hyperfine line of P@C_{60} can be observed due the second order hyperfine splitting. Even for nutation pulses as long as t_p = 700 ns the frequency width of the pulse covers the whole hyperfine line. Only for an applied magnetic field as small as B_1 = 11 µT, corresponding to $t(\pi/2)$ = 832 ns, off–resonant components in the nutation frequency were observed at 1 MHz. In a quantum computing scheme with a large interaction between the qubits, the separation between the finestructure lines would be large and off–resonant excitation has to be considered.

For two P@C_{60} powder samples, the transient nutation has been used to analyse the spectra. At room temperature as well as at T = 10 K, a zero–field splitting (zero–field splitting) has been found as evidenced by a change of the nutation frequency for low magnetic fields B_1. From the dependence of the rotation frequency with respect to the

applied field, the zero–field splitting has been estimated as $D/g_e\mu_B \sim 240$ µT at room temperature and $D/g_e\mu_B > 400$ µT at T = 10 K.

Echo-detected spectra measured at low temperatures indeed reveal a splitting of the fine structure transitions. However, the (±3/2, ±1/2) transitions are much too broad for the estimated zero–field splitting. A distribution of D values was discussed as the likely explanation. Crystal–field distortions of the fullerene cage are known to cause a small zero–field splitting in N@C_{60} $D/g_e\mu_B \sim 20$ µT. To explain the broad lines of P@C_{60}, this effect and its variation would have to be stronger by an order of magnitude compared to N@C_{60}.

All of the effects due to zero–field splitting measured for P@C_{60} in solid state with transient nutation will be valid for chemical modifications of N@C_{60} that have a large zero–field splitting, as well.

It has been demonstrated that, without any refocusing, about 50 single qubit operations can be done with N@C_{60} at room temperature. Up to 30 oscillations could be observed for P@C_{60}. This is sufficient for the implementation of short quantum algorithms.